

Optical Properties of LiNbO₂ Thin Films


A PREPRINT

T. Kurachi
Far-IR R&D Center
University of Fukui
Fukui 910-8507, Japan

T. Yamaguchi
Far-IR R&D Center
University of Fukui
Fukui 910-8507, Japan

E. Kobayashi
Advanced Interdisciplinary Science & Technology
University of Fukui
Fukui 910-8507, Japan

 **T. Soma**
Department of CS&E
Tokyo Institute of Technology
Tokyo 152-8552, Japan

 **A. Ohtomo**
Department of CS&E
Tokyo Institute of Technology
Tokyo 152-8552, Japan

 **T. Makino**
Far-IR R&D Center
University of Fukui
Fukui 910-8507, Japan
tmakino@u-fukui.ac.jp

October 30, 2023

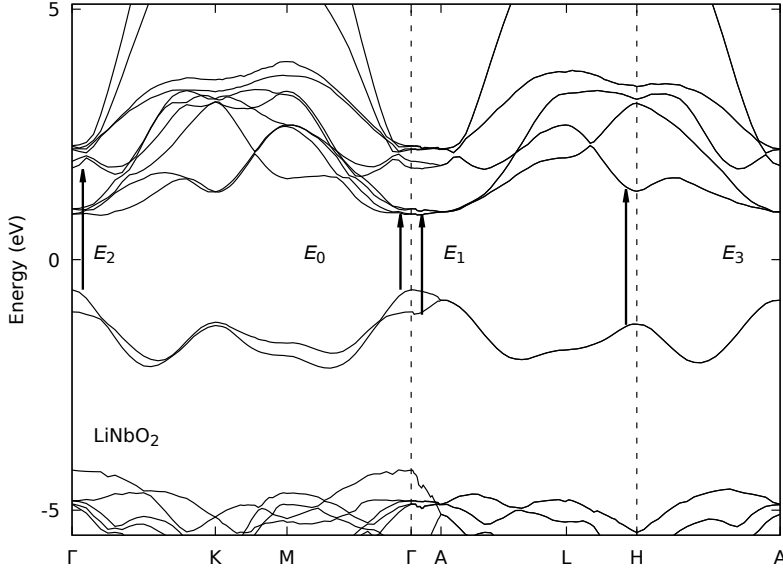
ABSTRACT

The complex dielectric functions of LiNbO₂ were determined using optical transmittance and reflectance spectroscopies at room temperature. The measured dielectric function spectra reveal distinct structures at several bandgap energies. The bandgaps (exciton resonances) in the spectrum were observed at *ca.* 2.3, 3.2, 3.9, and 5.1 eV, respectively. These experimental data have been fit using a model dielectric function based on the electronic energy-band structure near critical points plus excitonic effects. The features of measured dielectric functions are, to some extent, reproduced quantitatively by an *ab-initio* calculation including the interaction effects between electrons and holes.

1 1. Introduction

Lithium niobate is a member of the transition-metal oxide compounds. At normal temperature and pressure, it crystallizes in a form of three-dimensional LiNbO₃. Lithium niobate can also crystallize in the layered LiNbO₂ (LNO) modification, although it is metastable under normal conditions [1-2]. By using the epitaxial growth techniques such as pulsed laser deposition, it is now possible to grow LiNbO₂ thin films without the need for rather restricted conditions such as a reducing atmosphere [3-6]. This compound is known to be several intriguing properties such as the superconductivity [7-10] in the delithiated phase at approximately 5 K and the high ionic conductivity suitable for potential applications as a battery material [11-13].

Although stoichiometric LNO is a “mother material” of the delithiated counterpart having compatibility of transparency and the superconductivity, the little is known about the optical response of this compound. LNO is a direct gap semiconductor [14-17]. The bandgap energies were evaluated to be *ca.* 2.0 eV both experimentally [18] and theoretically [14]. On the other hand, the nature of these optical transitions has not been clarified yet for this material. This is partly because the experimental information is based on a diffused reflectance spectrum taken on a specimen in powdered form [18]. In this case, the conversion to the dielectric functions is very difficult. Generally, to draw electronic-structure-related knowledge from measured data, analysis based on the standard critical point (SCP) modeling [19] has been adopted so far. According to the SCP theory, the lineshape is considered to reflect that of the spectral distribution in the joint density of states of the valence and conduction bands. The lineshape of the joint density of states strongly depends on the dimensionality and the Lynch index which corresponds to the number of negative components in the effective mass vectors. Gaining insight into the nature of the optical transitions is attributed to the determination of the parameters such as the dimensionality and the Lynch index. Such a parameterization has not been, however, done so far for this material. These knowledges are very important for *e.g.* device applications.

Figure 1: Electronic energy-band structure of LiNbO₂.

In this work, we study the optical properties of LNO thin films. We present dielectric function spectra deduced from transmission and reflectance spectra at room temperature (RT) between 1.5 and 6.5 eV. A method is also described for calculating the spectroscopic distribution of the dielectric function of LNO where the relevant models are connected with the electronic energy-band structures of the compound. For comparison, we also show *ab-initio* calculation results with the *GW* level under linear-response approximations.

2 Theoretical Model

2.1 Electronic energy-band structure of LiNbO₂

Several groups have reported the calculated results on the electronic-energy band structures in LNO [14-17]. We also executed local-density approximation (LDA) calculations by ourselves. The reproducible results are obtained as shown in Fig. 1. To ensure computing cost-effectiveness for regression analysis, we attempted to reproduce the measured dielectric functions with critical points (CP's), the number of which is as small as possible. From the model-dielectric-function (MDF)-based regression analysis for the measured data, the energies of the CP's were evaluated to be *ca.* 2.3, 3.2, 3.9, and 5.1 eV. These transition energies are shown in Fig. 1 with vertical arrows and are labeled as E_0 , E_1 , E_2 , and E_3 . It should be noted that, for the assignments of the vertical arrows in Fig. 1, we looked for the corresponding direct transitions lower in energy if we could not find a transition having the same energy with the experiment. In the analysis, we neglect the following aspects for simplicity: (1) transitions above the E_3 gap, (2) the contributions from indirect transitions due to their extremely weaker nature in their intensities, and (3) the spin-orbit effects and the related splitting of the bands (conventionally denoted as Δ in the literature).

2.2 Model dielectric functions

We performed the line-shape analysis using the MDF approach [20]. Here, we summarize dielectric functions as a form of a complex function. To obtain $\epsilon_1(\omega)$, one can take its real parts, while for $\epsilon_2(\omega)$, imaginary parts should be taken.

The E_0 , E_1 , E_2 CP's may be of the three-dimensional (3D) M_1 type. The index i in the M_i notation corresponds to earlier-mentioned Lynch index. As shown in Fig. 2, the overall feature of the $\epsilon_1(\omega)$ spectrum is characterized with monotonically decreasing behavior concerning the photon energy, accompanied with optical anomalies at the CP's. To reproduce this behavior, the assumption of M_1 type is more appropriate. Because the M_1 CP's longitudinal effective mass is much larger than its transverse counterpart, one can treat these 3D M_1 CP's as a two-dimensional (2D) minimum M_0 . It is known that the equation in the approximation of the 2D M_0 CP gives a series of Wannier-type excitons if taking the excitonic effects into account [21]. In other words, one can neglect the one-electron contribution to the dielectric function in the case of the 3D M_1 CP. Due to its layered structure, LNO is expected to be a material where the electron-hole correlations are rather strong. Rough calculation on the binding energy of the Wannier-type exciton

yielded in *ca.* 70 meV for LNO by using the reported reduced effective mass ($0.57 m_0$) and background dielectric constant of *ca.* 10.3 [14]. The notation m_0 means electron's mass in rest. Besides, the excitonic effect could not be neglected in the case of 3D M_1 (2D M_0) CP for many elemental and compound semiconductors [20,22-25]. Thus, we can justifiably take this effect into account for the analysis. For *e.g.* the E_0 feature, the contribution of these excitons to $\epsilon(\omega)$ can be now written with Lorentzian lineshape as:

$$\epsilon(\hbar\omega) = \sum_{n=1}^{\infty} \frac{1}{(2n-1)^3} \left(\frac{A_0}{-i\Gamma_1 + E_0 - G_0/(2n-1)^2 - \hbar\omega} \right) \quad (1)$$

where A_0 is a constant corresponding to the strength parameter, E_0 is the energy of the CP, G_0 is the 2D binding energy of exciton. The value of Γ_0 is the broadening parameter. Because the ground-state exciton term occupies almost 95% of the total oscillator strength, we neglected the excited-state terms ($n \geq 2$) in the current analysis.

The E_3 peak is difficult to analyze as it does not correspond to a single, well defined CP. Thus, the E_3 structure has been characterized as a damped harmonic oscillator:

$$\epsilon(\hbar\omega) = \frac{A_3}{1 - \chi_3^2 - i\Gamma_3\chi_3} \quad (2)$$

with $\chi_3 = E/E_3$, where A_3 is the strength parameter and Γ_3 is a dimensionless broadening parameter.

3 Experimental and Calculation Procedures

LNO thin films were grown on MgAl₂O₄ (111) substrates using pulsed laser deposition (PLD) method with KrF excimer laser. The growth was conducted in vacuum at RT. After deposition, the films were annealed *in situ* at substrate temperature of 800 °C under a chamber pressure of 0.1 mtorr set by continuous flow of Ar/H₂ gas. Films were capped by several-nanometer-thick alumina films using PLD at RT in vacuum for avoiding reactions with air. The description of detailed growth process can be found elsewhere [6]. The film thickness is approximately 150 nm.

Optical transmittance and reflectance were measured with an ultraviolet-visible spectrometer at RT. Then, we converted these spectral intensities to those of the complex dielectric functions [26]. Here, the refractive index of the substrate is assumed to be independent of the photon energy because the bandgap of MgAl₂O₄ is significantly wider than the maximum energy of the measurement range (*i.e.*, 6.5 eV).

Structural information of LNO has been reported by several experimental groups, leading to the assignment of space group $P6_3/mmc$ (No. 194). We performed *ab-initio* calculation using the plane-wave basis set PWscf package of Quantum ESPRESSO [27-28] to evaluate the electronic-energy-band structures. For the lattice constant of LiNbO₂, $a=2.938$ Å and $c=10.596$ Å were used. The 3D Brillouin zone was integrated using a $7 \times 7 \times 2$ k-point grid. We have set the energy cutoff for the plane-wave basis to 30 Ry, and have used the Perdew–Burke–Ernzerhof (PBE) functional, which belongs to the class of generalized gradient approximation (GGA) functionals. In previous works, similar calculations have been made [14-15], and qualitatively coincided results could be obtained by ourselves. For the optical spectra calculations such as dielectric functions, we used Respack *ab-initio* package [29-30]. This package solves Bethe-Salpeter-like equations numerically under single-excitation configuration-interaction (SECI) treatment. By doing that, the interactions between electrons and holes are taken into account.

4 Results and Discussion

In Fig. 2, we plot the real (ϵ_1) and imaginary (ϵ_2) parts of dielectric function spectra $\epsilon(\omega)$ of LNO determined at RT. As seen in the figure, the experimental data reveal clear structures at the 2.2 to 2.4-eV region. This structure originates from transition at the E_0 edge. The structures appearing at the 3.0 to 3.4, 3.6 to 4.2, and 4.7 to 5.5-eV regions are due to the E_1 , E_2 , and E_3 transitions, respectively.

The model dielectric function (MDF) approach given in Sec. IIB was used to fit the experimental dispersion of $\epsilon(\omega)$ over the entire range of the measurements (0 to 6.5 eV). The parameters such as A_0 and A_1 are used as adjustable constants for the calculations of $\epsilon_1(\omega)$ and $\epsilon_2(\omega)$. As has been already mentioned in Sec. IIB, the $\epsilon_1(\omega)$ for LNO is, in overall, a monotonically decreasing function with upward convex in 1.5 to 5-eV range except for several optical anomalies such as E_0 . This is very peculiar compared to those for many other elemental and compound semiconductors [20,22-25]. This is somehow reminiscent of that in α -Sn [24]. In this case, very strong absorption band is present in the ϵ_2 spectrum, giving rise to consistent explanation in terms of the 3D M_0 CP with very large transition strength. This is

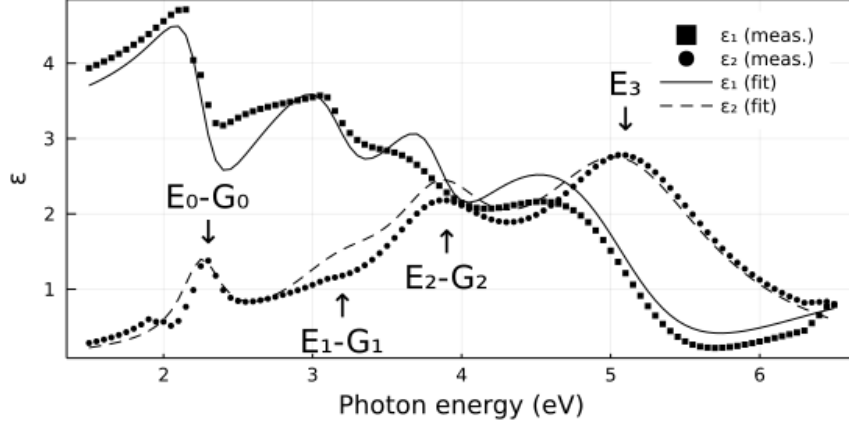


Figure 2: Real (squares) and imaginary (circles) parts of the dielectric functions of LNO thin film taken at RT. The symbols are the experimental data, while the lines are calculated for real (solid) and imaginary (dashed) parts using Eq. (1), Eq. (2), and $\epsilon_{1\infty} = 2$.

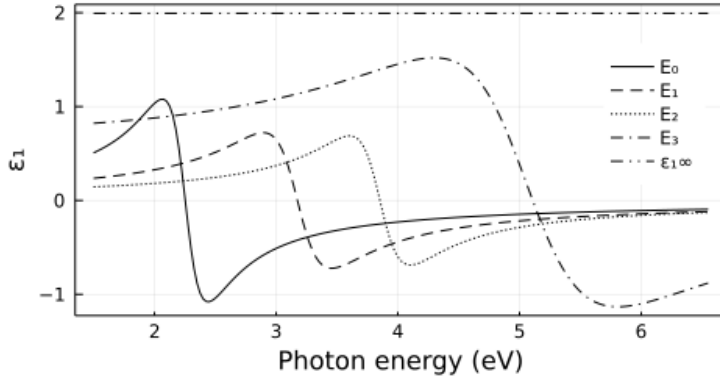


Figure 3: Individual contribution to imaginary part of dielectric function of the various energy gaps for LNO. They are obtained from Eq. (1) for the M_1 (i.e., the 2D-exciton) contribution, and from Eq. (2) for the E_3 -gap contribution.

not the case for LNO. To reproduce the ϵ_1 behavior, there seems no other solution except for positive adoption of the M_1 -type CP even for the lowest energy gap because the difference between the ϵ_1 values at both ends is larger in the case of 3D M_1 (2D M_0). Comparison of the behavior at both ends revealed us that the lineshape of the 2D M_0 MDF is known to drop significantly, while that of the 3D M_0 MDF remains relatively flat [20]. Therefore, the 2D M_0 MDF is more suitable to reproduce the overall ϵ_1 tendency. The experimental data on $\epsilon_1(\omega)$ turned out to be still somehow larger than the model fit. To improve this fit, we then introduced a phenomenological term $\epsilon_{1\infty}$ in addition to $\epsilon_1(\omega)$ to account for the contributions from higher-lying energy gaps. This term $\epsilon_{1\infty}$ is assumed to be nondispersive.

The solid and dashed lines in Fig. 2 are obtained from the sum of Eqs. (1) and (2), and $\epsilon_{1\infty}=2.0$. The vertical arrows in the figure indicate the excitonic peak energies (E_0-G_0 , E_1-G_1 , E_2-G_2) and the positions of the CP (E_3). The best-fit parameters are listed in Table I. Due to the earlier-mentioned assumptions, we could not determine the excitonic binding energies such as G_0 experimentally. Individual contributions to the dielectric functions of the various energy gaps for LNO are shown in Figs. 3 and 4, respectively. They are obtained from Eq. (1) for the 2D-exciton contribution in the E_0 , E_1 , and E_2 regions, and from Eq. (2) for the E_3 gap contribution.

The sums of Eqs. (1) and (2) fit the main features of the ϵ_1 and ϵ_2 data, but the agreement with the experiment is rather qualitative. The difference probably could come from several sources, including (1) the Lorentz approximation for

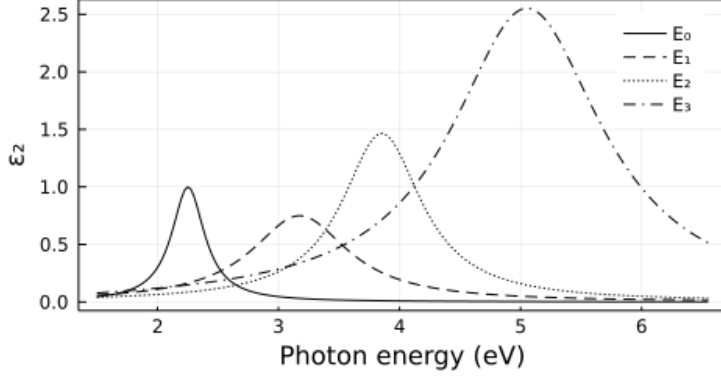
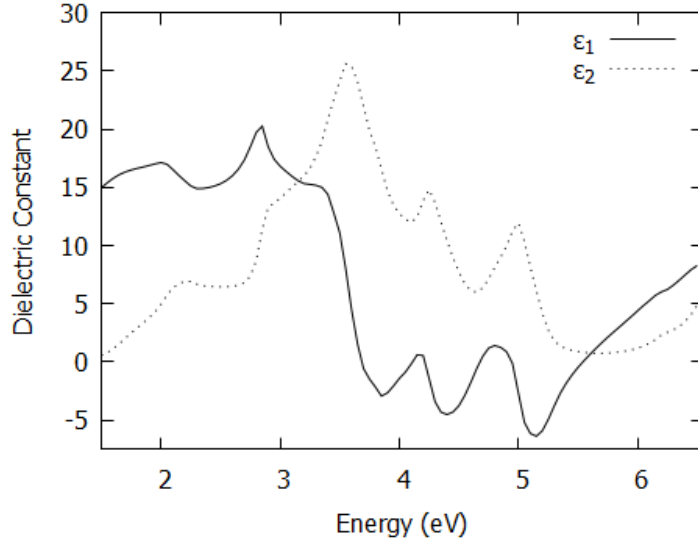


Figure 4: As of Fig. 3, but for real part.

Figure 5: Real and imaginary parts of the dielectric functions of LNO, obtained from the *ab-initio* calculation.

broadening (which is known to give too much absorption below direct band edges [31]), (2) the neglect for the excited-states excitons [20], or (3) the parabolic assumption of the CP's [19].

As understood from the table, some of the best-fit parameters from the ϵ_1 analysis are different from the ϵ_2 counterparts. Being compliant with SCP theory's policy, we took the average from these values, as shown in this figure. We believe that these averaged values should be material parameters of LNO. An increase in the number of MDF's (CP's) is expected to lead to an improved agreement with the experiment, even with the same (common) values on the parameters. However, it might be an excessive assumption to include an additional transition to the position where no peak or anomaly is observed. Indeed, this might be justified by the fact that calculated SECI spectra include at least five CP's in the energy range (1.5 to 6.5 eV), as can be viewed from Fig. 5.

Neglecting contributions from the optical anomalies, overall $\epsilon_1(\omega)$ in the SECI spectrum is a monotonically decreasing function with upward convex in the 1.5 to 4-eV range. This feature is in good agreement with the experiment. Besides, the agreement on the E_0 energy is also good. According to the *ab-initio* calculation under the LDA level, the bandgap energy is evaluated to be approximately 1.5 eV. The calculated energy is significantly lower than that of experimental value (*ca.* 2.3 eV). As is often the case, it is well-known that the LDA level calculation tends to underestimate the bandgap energy. On the other hand, the *ab-initio* SECI calculation considers the electron-hole interaction (excitonic) effects in this material, leading to the improved agreement with the experiment. The spectral blue-shift from the

Table 1: Table I: Material parameters used in the calculation of the optical constants of LNO.

Parameters	Values from ϵ_1	Values from ϵ_2	Average
E_0 (eV)	2.25	2.28	2.27
Γ_0 (eV)	0.19	0.17	0.18
A_0 (eV)	0.41	0.17	0.29
E_1 (eV)	3.18	3.18	3.18
Γ_1 (eV)	0.28	0.49	0.39
A_1 (eV)	0.41	0.37	0.39
E_2 (eV)	3.85	3.85	3.85
Γ_2 (eV)	0.25	0.40	0.33
A_2 (eV)	0.34	0.59	0.47
E_3 (eV)	5.1	5.2	5.2
Γ_3	0.3	0.3	0.3
A_3	0.76	0.75	0.76
$\epsilon_{1\infty}$	2		2

LDA-level result is probably due to the so-called self-energy effect. Furthermore, the energetic positions of E_1 and E_3 CP's are in reasonable agreement with the experiment.

We notice that the calculated spectra structures are sharper and more distinct than those in the measured one. The calculated $\epsilon_1(\omega)$ amplitude as defined by the difference of the ϵ_1 value at 1.5 and 6.5 eV is also larger. These looser agreements are probably related to the same origin. The broadening parameter corresponding to the width of the Green functions used in the calculation is significantly smaller than that obtained in the measurement. The doublet splitting of the E_2 is observed in the SECI spectra. Experimentally, the double seems not resolved due to the broadening effect. Thus, our results should stimulate further work for this material both experimentally and theoretically.

Finally, we mention refractive-index dispersion in the transparency region. As seen in Fig. 2, the analysis results are in agreement with the experiment (ϵ_1) over the entire range of photon energies. On the other hand, the agreement is looser. An increase in the parameter $\epsilon_{1\infty}$ from 2 to 3.5 improves the agreement in the transparency region. However, this does not give a satisfactory fit to the experimental data at higher photon energies (> 3.0 eV). Several research groups have reached a similar conclusion on GaP, AlSb, and ZnSe. The looser agreement is probably related to the earlier-mentioned Lorentz approximation for broadening [20,32-33]. Indeed, Pollak's group has introduced a phenomenological linear cutoff to eliminate this problem giving too much absorption below direct band edges [31]. We did not attempt this here because the cutoff's adoption forced us a numerical Kramers-Kronig conversion to the ϵ_1 counterpart, thus making it impossible to analyze the experimental data within the regression analysis framework based on a conventional Levenberg-Marquardt algorithm.

5 Conclusion

In summary, we have reported the dielectric functions of LNO around the fundamental band gap E_0 (ca. 2.3 eV) and up to 6.5 eV for RT. The observed spectra reveal distinct structures at energies the E_0 , E_1 , E_2 and E_3 CP's. These data are analyzed based on a simplified model of the interband transitions, including these transitions as the main dispersion mechanisms. The analyzed results are in qualitative agreement with the experiment. Many important material parameters of these transitions were determined. The comparison was made with the results of *ab-initio* calculations, taking the electron-hole correlation effects into account.

6 Acknowledgments

T.M. wishes to thank the financial support of the Ministry of Education, Culture, Sports, Science and Technology Grant No. KAKENHI-19K05303. This work was partially supported from No. KAKENHI-20K15169. All of the *ab-initio* calculations were performed in the Supercomputer Center at the Institute of Solid-State Physics, the University of Tokyo.

7 References

[1] G. Meyer, R. Hoppe, The first oxoniobate LiNbO₂, *Angew. Chem. Int. Ed.* 13 (1974) 744–745. <https://doi.org/10.1002/anie.197407441>.

- [2] N. Kumada, S. Muramatu, F. Muto, N. Kinomura, S. Kikkawa, M. Koizumi, Topochemical reactions of LiNbO₂, *J. Solid State Chem.* 73 (1988) 33–39. [https://doi.org/10.1016/0022-4596\(88\)90050-3](https://doi.org/10.1016/0022-4596(88)90050-3).
- [3] N. Sarmadian, R. Saniz, B. Partoens, D. Lamoen, Easily doped p-type, low hole effective mass, transparent oxides, *Sci. Reports.* 6 (2016) 20446. <https://doi.org/10.1038/srep20446>.
- [4] W.E. Henderson, W.L. Calley, A.G. Carver, H. Chen, W.A. Doolittle, A versatile metal-halide vapor chemistry for the epitaxial growth of metallic, insulating and semiconducting films, *J. Cryst. Growth.* 324 (2011) 134–141. <https://doi.org/10.1016/j.jcrysgro.2011.03.049>.
- [5] M.B. Tellekamp, J.C. Shank, W.A. Doolittle, Molecular beam epitaxy of lithium niobium oxide multifunctional materials, *J. Cryst. Growth.* 463 (2017) 156. <https://doi.org/10.1016/j.jcrysgro.2017.02.020>.
- [6] T. Soma, K. Yoshimatsu, A. Ohtomo, P-type transparent superconductivity in a layered oxide, *Science Adv.* 6 (2020) eabb8570. <https://doi.org/10.1126/sciadv.abb8570>.
- [7] M.J. Geselbracht, T.J. Richardson, A.M. Stacy, Superconductivity in the layered compound LiNbO₂, *Nature (London).* 345 (1990) 324. <https://doi.org/10.1038/345324a0>.
- [8] M.A. Rzeznik, M.J. Geselbracht, M.S. Thompson, A.M. Stacy, Superconductivity and phase separation in NaNbO₂, *Angew. Chem. Int. Ed.* 32 (1993) 254–255. <https://doi.org/10.1002/anie.199302541>.
- [9] E.G. Moshopoulou, P. Bordet, J.J. Capponi, Superstructure and superconductivity in LiNbO₂ single crystals, *Phys. Rev. B.* 59 (1999) 9590–9599. <https://doi.org/10.1103/physrevb.59.9590>.
- [10] G.T. Liu, J.L. Luo, Z. Li, Y.Q. Guo, N.L. Wang, D. Jin, T. Xiang, Evidence of s-wave pairing symmetry in the layered superconductor LiNbO₂ from specific heat measurements, *Phys. Rev. B.* 74 (2006). <https://doi.org/10.1103/physrevb.74.012504>.
- [11] J.D. Greenlee, C.F. Petersburg, W.L. Calley, C. Jaye, D.A. Fischer, F.M. Alamgir, W.A. Doolittle, In-situ oxygen x-ray absorption spectroscopy investigation of the resistance modulation mechanism in LiNbO₂ memristors, *Appl. Phys. Lett.* 100 (2012) 182106. <https://doi.org/10.1063/1.4709422>.
- [12] S.A. Howard, C.N. Singh, G.J. Paez, M.J. Wahila, L.W. Wangoh, S. Sallis, K. Tirpak, Y. Liang, D. Prendergast, M. Zuba, J. Rana, A. Weidenbach, T.M. McCrone, W. Yang, T.-L. Lee, F. Rodolakis, W. Doolittle, W.-C. Lee, L.F.J. Piper, Direct observation of delithiation as the origin of analog memristance in LiNbO₂, *APL Materials.* 7 (2019) 071103. <https://doi.org/10.1063/1.5108525>.
- [13] X. Xu, G. Liu, S. Ni, J.T.S. Irvine, Layered lithium niobium oxide LiNbO₂ as a visible-light-driven photocatalyst for H₂ evolution, *J. Phys.: Energy.* 1 (2018) 015001. <https://doi.org/10.1088/2515-7655/aad4be>.
- [14] E.R. Ylvisaker, W.E. Pickett, First-principles study of the electronic and vibrational properties of LiNbO₂, *Phys. Rev. B.* 74 (2006) 075104. <https://doi.org/10.1103/physrevb.74.075104>.
- [15] D.L. Novikov, V.A. Gubanov, V.G. Zubkov, A.J. Freeman, Electronic structure and electron-phonon interactions in layered Li_xNbO₂ and Na_xNbO₂, *Phys. Rev. B.* 49 (1994) 15830. <https://doi.org/10.1103/physrevb.49.15830>.
- [16] K.-W. Lee, J. Kunes, R.T. Scalettar, W.E. Pickett, Correlation effects in the triangular lattice single-band system Li_xNbO₂, *Phys. Rev. B.* 76 (2007) 144513. <https://doi.org/10.1103/physrevb.76.144513>.
- [17] J.U. Rahman, N.V. Du, G. Rahman, V.M. Garcia-Suarez, W.-S. Seo, M.H. Kim, S. Lee, Localized double phonon scattering and DOS induced thermoelectric enhancement of degenerate nonstoichiometric LiNbO₂ compounds, *RSC Advances.* 7 (2017) 53255. <https://doi.org/10.1039/c7ra10557f>.
- [18] M.J. Geselbracht, A.M. Stacy, A.R. Garcia, B.G. Silbernagel, G.H. Kwei, Local environment and lithium ion mobility in lithium niobate LiNbO₂: Inferences from structure, physical properties, and NMR, *J. Phys. Chem.* 97 (1993) 7102. <https://doi.org/10.1021/j100129a030>.
- [19] S. Loughin, R. French, L. DeNoyer, W.-Y. Ching, Y.-N. Xu, Critical point analysis of the interband transition strength of electrons, *J. Phys. D.* 29 (1996) 1740. <https://doi.org/10.1088/0022-3727/29/7/009>.
- [20] S. Adachi, T. Taguchi, Optical properties of ZnSe, *Phys. Rev. B.* 43 (1991) 9569. <https://doi.org/10.1103/PhysRevB.43.9569>.
- [21] Y. Petroff, M. Balkanski, Coulomb effects at saddle-type critical points in CdTe, ZnTe, ZnSe, and HgTe, *Phys. Rev. B.* 3 (1971) 3299. <https://doi.org/10.1103/physrevb.3.3299>.

- [22] S. Adachi, Model dielectric constants of GaP, GaAs, GaSb, InP, InAs, and InSb, *Phys. Rev. B.* 35 (1987) 7454. <https://doi.org/10.1103/PhysRevB.35.7454>.
- [23] S. Adachi, Model dielectric constants of si and ge, *Phys. Rev. B.* 38 (1988) 12966. <https://doi.org/10.1103/PhysRevB.38.12966>.
- [24] S. Adachi, Optical properties of alpha-sn, *J. Appl. Phys.* 66 (1989) 813. <https://doi.org/10.1063/1.343502>.
- [25] S. Ninomiya, S. Adachi, Optical properties of cubic and hexagonal CdSe, *J. Appl. Phys.* 78 (1995) 4681. <https://doi.org/10.1063/1.359815>.
- [26] R.E. Denton, R.D. Campbell, S.G. Tomlin, The determination of the optical constants of thin films from measurements of reflectance and transmittance at normal incidence, *J. Phys. D.* 5 (1972) 852. <https://doi.org/10.1088/0022-3727/5/4/329>.
- [27] P. Giannozzi, S. Baroni, N. Bonini, M. Calandra, R. Car, C. Cavazzoni, D. Ceresoli, G.L. Chiarotti, M. Cococcioni, I. Dabo, A.D. Corso, S. de Gironcoli, S. Fabris, G. Fratesi, R. Gebauer, U. Gerstmann, C. Gougoussis, A. Kokalj, M. Lazzeri, L. Martin-Samos, N. Marzari, F. Mauri, R. Mazzarello, S. Paolini, A. Pasquarello, L. Paulatto, C. Sbraccia, S. Scandolo, G. Sclauzero, A.P. Seitsonen, A. Smogunov, P. Umari, R.M. Wentzcovitch, QUANTUM ESPRESSO: A modular and open-source software project for quantum simulations of materials, *J. Phys.: Cond. Mat.* 21 (2009) 395502. <https://doi.org/10.1088/0953-8984/21/39/395502>.
- [28] P. Giannozzi, O. Andreussi, T. Brumme, O. Bunau, M.B. Nardelli, M. Calandra, R. Car, C. Cavazzoni, D. Ceresoli, M. Cococcioni, N. Colonna, I. Carnimeo, A.D. Corso, S. de Gironcoli, P. Delugas, R.A.D. Jr, A. Ferretti, A. Floris, G. Fratesi, G. Fugallo, R. Gebauer, U. Gerstmann, F. Giustino, T. Gorni, J. Jia, M. Kawamura, H.-Y. Ko, A. Kokalj, E. Kucukbenli, M. Lazzeri, M. Marsili, N. Marzari, F. Mauri, N.L. Nguyen, H.-V. Nguyen, A. Otero-de-la-Roza, L. Paulatto, S. Ponce, D. Rocca, R. Sabatini, B. Santra, M. Schlipf, A.P. Seitsonen, A. Smogunov, I. Timrov, T. Thonhauser, P. Umari, N. Vast, X. Wu, S. Baroni, Advanced capabilities for materials modelling with QUANTUM ESPRESSO, *J. Phys.: Cond. Mat.* 29 (2017) 465901. <https://doi.org/10.1088/1361-648X/aa8f79>.
- [29] K. Nakamura, Y. Yoshimoto, R. Arita, S. Tsuneyuki, M. Imada, Optical absorption study by ab initio downfolding approach: Application to GaAs, *Phys. Rev. B.* 77 (2008) 195126. <https://doi.org/10.1103/physrevb.77.195126>.
- [30] K. Nakamura, Y. Yoshimoto, Y. Nomura, T. Tadano, M. Kawamura, T. Kosugi, K. Yoshimi, T. Misawa, Y. Motoyama, RESPACK: An ab initio tool for derivation of effective low-energy model of material, arXiv:2001.02351. (2020). <https://arxiv.org/abs/2001.02351>.
- [31] T. Holden, P. Ram, F.H. Pollak, J.L. Freeouf, B.X. Yang, M.C. Tamargo, Spectral ellipsometry investigation of ZnCdSe lattice matched to InP, *Phys. Rev. B.* 56 (1997) 4037–4046. <https://doi.org/10.1103/PhysRevB.56.4037>.
- [32] K. Strössner, S. Ves, M. Cardona, Refractive index of GaP and its pressure dependence, *Phys. Rev. B.* 32 (1985) 6614. <https://doi.org/10.1103/physrevb.32.6614>.
- [33] S. Zollner, C. Lin, E. Schönher, A. Böhringer, M. Cardona, The dielectric function of AlSb from 1.4 to 5.8 eV determined by spectroscopic ellipsometry, *J. Appl. Phys.* 66 (1989) 383. <https://doi.org/10.1063/1.343888>.